Analysis of Aft-Control Surface Interaction with an Axisymmetric Underwater Vehicle Hull

David Kirkby, Australian Maritime College & ENSE[3], David.Kirkby@dst.defence.gov.au
David A. Pook, RMIT, David.Pook@dst.defence.gov.au
Martin Renilson, Pacific ESI, martin@renilson-marine.com
Dev Ranmuthugala, DST, Dev.Ranmuthugala2@dst.defence.gov.au

ABSTRACT

Aft-Control-Surfaces (ACSs) provide underwater vehicles with the forces and moments required to maintain stability, and control manoeuvres. Thus, accurate prediction of ACS hydrodynamic loads is essential to adequately size the control surfaces and to predict the vehicle's stability and control characteristics. Undersized control surfaces may result in failure to meet manoeuvring requirements or provide insufficient directional and pitch stability. Over-sized control surfaces can adversely affect other aspects of the vehicle such as resistance and acoustic signature.

Sizing ACSs requires consideration of the hydrodynamic interaction with the vehicle's hull. The presence of the hull alters the normal force produced by an ACS when compared to the ACS geometry as an isolated wing exposed to the freestream. The ratio of these two conditions is referred to as the ACS efficiency (or tailplane efficiency). Lyons and Bisgood [1] provide a methodology to estimate hull effects on the ACS normal force curve slope. Dempsey [2] experimentally determined the effect of a tear-drop shaped hull on the ACS normal force curve slope for a range of ACS geometries. The Dempsey experiment showed a greater hull influence than predicted by the Lyons and Bisgood method. Bettle [3] and Mackay, Watt and Bohlmann [4] have suggested this might be due to Reynolds number effects.

In this paper, the possible Reynolds number effects were investigated by simulating the Dempsey [2] experiment using Computational Fluid Dynamics (CFD) that solved the Reynolds Averaged Navier-Stokes (RANS) equations. Standard RANS modelling techniques that assume all turbulent flow produced results in good agreement with the relatively low Reynolds number data of Dempsey, thereby discounting significant laminar boundary layer effects. Dempsey's experiment was simulated at higher Reynolds numbers and ACS efficiency was found to be dependent on the Reynolds Number. The choice of turbulence closure model in the RANS simulations was found to affect the prediction of ACS efficiency. The CFD results confirm the suitability of using Dempsey's data for predicting ACS efficiency at model scale Reynolds numbers for an underwater vehicle hull with relatively shallow stern angles.

INTRODUCTION

The control surfaces of an underwater vehicle, in conjunction with its movable ballast, and propulsor form the basis of the vehicle's control system. During the initial design phase, design of the control system is highly iterative and considers a large number of design alternatives [4]. Analysis of each iteration using model scale testing or numerical methods, such as Computational Fluid Dynamics (CFD), would be inefficient and prohibitively expensive. Consequently, it is advantageous that valid empirical predictions of the vehicle's control system are available to a designer during the preliminary design phase.

The positioning of the Aft Control Surfaces (ACSs) and their interaction with the hull results in reduced hydrodynamic loading when compared to the ACS geometry considered as an isolated wing exposed to the freestream. Integration of the ACS with the hull reduces the effective ACS normal force curve slope relative to an isolated ACS geometry. The ratio of the integrated ACS normal force curve slope and the ACS isolated lift curve slope is referred to as the ACS efficiency (or tailplane efficiency, K_{wb}),

$$K_{wb} = \frac{C_{Z,\alpha}}{C_{L,\alpha}} \tag{1}$$

where $C_{Z,\alpha}$ is the ACS normal force curve slope when integrated with the hull and $C_{L,\alpha}$ is the lift curve slope for the equivalent isolated ACS. Two widely used empirical methods for predicting ACS efficiency are Lyons and Bisgood [1] and Dempsey [2]. The results of Dempsey [2] show a much greater hull influence on the ACS lift curve slope and consequently a lower ACS efficiency, relative to the results of Lyons and Bisgood [1]. Bettle [3] and Mackay, Watt and Bohlmann [4] have suggested that the lower ACS efficiency predicted by the Dempsey [2] method is due to Reynolds number effects. Mackay, Watt and Bohlmann [4] proposed a critical Reynolds number (Re) threshold of approximately 10^6 (based on the ACS mean cord) above which efficiency tends toward the higher values of Lyons and Bisgood [1] and below which efficiency tends toward Dempsey's prediction. This proposed critical threshold, together with the lack of turbulence tripping on the ACS in Dempsey's experiment, suggests that laminar flow may be responsible for the reduced efficiency.

It is clear that there remains significant uncertainty in the empirical relationships used to predict ACS efficiency. This uncertainty limits their usefulness in the design of underwater vehicles. Appropriate sizing of control surfaces is critical for ensuring that the vehicle meets its manoeuvring requirements whilst minimising resistance and acoustic signature and it therefore remains an important area of research.

This study simulates the Dempsey [2] experiment using Reynolds Average Navier-Stokes (RANS) CFD to determine the suitability of Dempsey's empirical method for the prediction of underwater vehicle ACS efficiency. Investigations into the influence of turbulence modelling and Reynolds number on ACS efficiency are also presented.

THEORY

Dempsey [2] presented results in the body axis system with the origin at the body centre of buoyancy, as show in Figure 1. The normal forces were non-dimensionalised with,

$$Z' = \frac{2Z}{\rho L^2 U^2} \tag{2}$$

where Z is the normal force (in the body axis), L the hull length, ρ the fluid density, and U the freestream velocity.

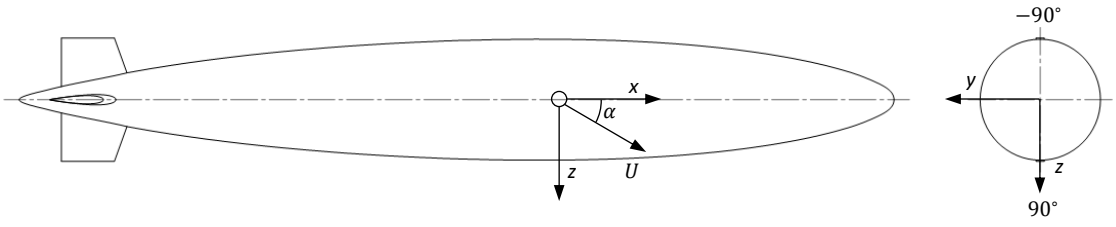

Figure 1: Appended Dempsey geometry and body fixed coordinate system with the origin at the centre of buoyancy.

Dempsey [2] provides a detailed explanation of the calculation methods used to determine ACS efficiency. The lift curve slope for an isolated ACS ($C_{L,\propto}$,) is calculated using the relationship presented by Whicker and Fehlner [5],

$$C_{L,\propto} = \frac{1.8\pi a}{1.8+\cos(\varphi)\sqrt{\frac{a^2}{\cos^2(\varphi)}+4}} \tag{3}$$

where a is the ACS aspect ratio, and φ is the ACS sweep angle at 25% chord.

To determine the ACS lift curve slope when integrated with the hull, Dempsey [2] measured the normal forces of the unappended hull (Z'_h) and the hull with ACSs (Z'_{ha}). The contribution of the ACS to a change of the normal force with respect to a change of vertical velocity ($\Delta Z'_w$) is,

$$\Delta Z'_w = \frac{\Delta Z'_{ha}}{\Delta w'} - \frac{\Delta Z'_h}{\Delta w'} \tag{4}$$

where w' is the vertical velocity (w) non-dimensionalised by U. For small pitch angles (α),

$$w' \cong -\alpha \tag{5}$$

where α is in radians. The normal force curve slope can be expressed as [6],

$$C_{Z,\alpha} = C_{L,\alpha} + C_D \tag{6}$$

where C_D is the vehicle's drag coefficient. For small pitch angles, C_D for the appended and unappended geometries is approximately equal and therefore cancel in the calculation of the ACS normal force curve slope in (4). Hence, for small α, the ACS lift and normal force curve slopes are approximately equivalent (as assumed by [2]). The ACS normal force curve slope when integrated with the hull is given by,

$$C_{Z,\alpha} = -\Delta Z'_W \frac{L^2}{2A} \tag{7}$$

where the reference area (A) has been changed to the planform area of the ACS (see Figure 2). The choice of pitch angles will affect the calculation of the ACS lift curve slope. Dempsey [2] does not explicitly state the pitch angles used. However, using provided data for pitch angles of 0° and 2° gives the Dempsey calculated ACS efficiency. ACS efficiency was then calculated as the ratio of $C_{Z,\alpha}$ to that of an equivalent isolated control surface, $C_{L,\alpha}$, as defined by (1).

NUMERICAL MODEL

Geometry

Dempsey's [2] towing tank experiments used the Model 4621 hull. The hull had a length (L) of 4.572 m and a maximum diameter (D) of 0.6228 m. The centre of buoyancy was located 2.0373 m from the bow. A sand strip was used at x/L = 0.396 to trip the hull boundary layer; however no turbulence trip was used on the ACSs. The Model 4621 hull differs somewhat from the design of a modern underwater vehicle due to its tear drop shape, with no parallel mid-body, and a relatively shallow tail half-angle of approximately 6.5°.

Dempsey [2] tested 20 different trapezoidal ACS configurations (a combination of five chords, and four spans) appended to the Model 4621 hull to parametrically assess the influence of ACS aspect ratio on the stability derivatives and ACS efficiency. Of the four different spans assessed by Dempsey, the present work focuses on the results of the 'B' span. The B span was the largest span that did not exceed the maximum hull diameter [6] and was therefore considered the most relevant to the design of an underwater vehicle. Two different cords lengths were assessed, the '3' and '11' cords, which represented the maximum and minimum cord lengths tested by Dempsey [2]. Details of the two configurations are defined in Table 1 and a plan view of the Model 4621 afterbody, and a generic trapezoidal ACS is shown in Figure 2.

The various geometry configurations were modelled in CATIA V5. Three simplifications were made to simplify generation of the CFD mesh and improve mesh quality: the two struts mounting the hull to the towing carriage were not included (geometry of struts was not specified by Dempsey); the tail of the Model 4621 hull was shortened (not tapered to a point) with a 5 mm radius applied to remove the need for an axisymmetric pole in the CFD grid; and the trailing edges of the ACS were truncated by 5 mm, increasing the trailing edge thickness to approximately 2mm (the physical trailing edge thickness was not specified by Dempsey).

Table 1: ACS configurations from Dempsey [2] simulated in this study.

Configuration (Dempsey 1977)	Span b (m)	Tip Cord C_{TIP} (m)	Reference Area A (m^2)	Aspect Ratio ($\frac{2b^2}{A}$)	ACS Mean Body Diameter D_1 (m)
3B	0.3048	0.0762	0.04013	4.64	0.1551
11B	0.3048	0.2794	0.10206	1.82	0.2097

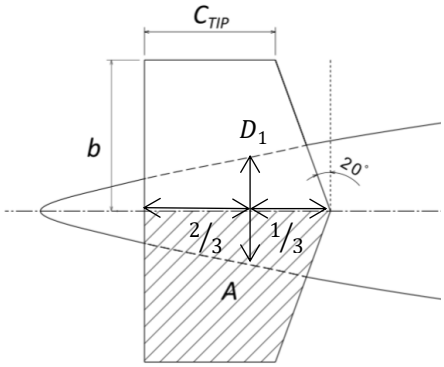

Figure 2: Plan view of Model 4621 afterbody showing a generic trapezoidal ACS with reference dimensions.

Fluid Domain

The fluid domain was composed of two sub domains, referred to as the inner and outer domains, joined by a non-conformal interface. This approach was used to reduce the mesh cell count and consequently the required computational resources. The inner domain extended $3D$ both forward and aft of the body and $3D$ away from the maximum diameter. The outer domain extended $3L$ forward of the body, $8L$ aft of the body, and $2L$ from the hull centreline. A mapped non-conformal interface boundary condition between the two domains was specified in the solver.

The boundary conditions at the extent of the outer domain are shown in Figure 3. Since the Dempsey experiment did not consider variation in yaw angle, the computational domain was symmetrical about the x-z plane. In order to reduce total mesh size a half model was simulated with a symmetry boundary condition imposed.

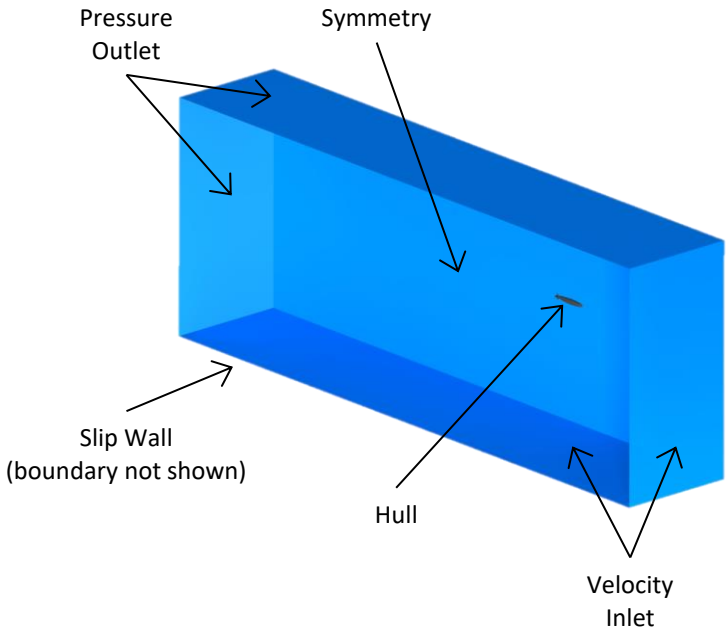

Figure 3: Fluid domain and boundary conditions

A velocity inlet was applied at the forward and lower boundaries of the domain. Specification of the u and w velocity components allowed for the hull to be considered at various pitch

angles (0-16°) without the need to re-mesh the geometry. A velocity magnitude corresponding to a tow speed of 6 knots was imposed to model the conditions of Dempsey's [2] experiments. The tow speed provides a hull Reynolds Number of 12.5×10^6 based on L, and an ACS mean cord Reynolds Number of 0.32 to 0.86×10^6 for the 3B and 11B configurations respectively.

The downstream and upper boundaries were set as pressure outlets. The hull and ACS walls were treated as non-slip walls. The far-field wall opposite the symmetry plane was modelled as a slip wall to simulate free-stream conditions. In Dempsey's [2] experiments, the model was towed at a depth of 3.05 m which was considered sufficiently deep to ignore free surface effects.

Mesh

A fully structured grid was utilised to discretise the fluid domain around both the unappended and appended Model 4621 hull. This approach provided two main advantages. Firstly a structured mesh reduces solution time, due to the reduced cell count (relative to a tetrahedral mesh) and through improved multigrid acceleration. In addition, structured grids have demonstrated reduced discretisation error on well aligned flows thereby increasing solution accuracy [7].

The structured grid was developed using Pointwise (18.2 R1) meshing software. Figure 4 shows the surface mesh for the appended hull. An O-H grid topology was used for both appended and un-appended geometries. O-grid topology enveloped the body to a distance of $1D$ from the body in order to adequately resolve near wall behaviour. H-grid topology was then extended to the boundaries of the inner domain. The grid for the outer domain was consistent for all simulations, while the grid for the inner domain was varied to account for the different geometries. A non-dimensional wall distance (y^+) of order 1 was maintained for all RANS simulations.

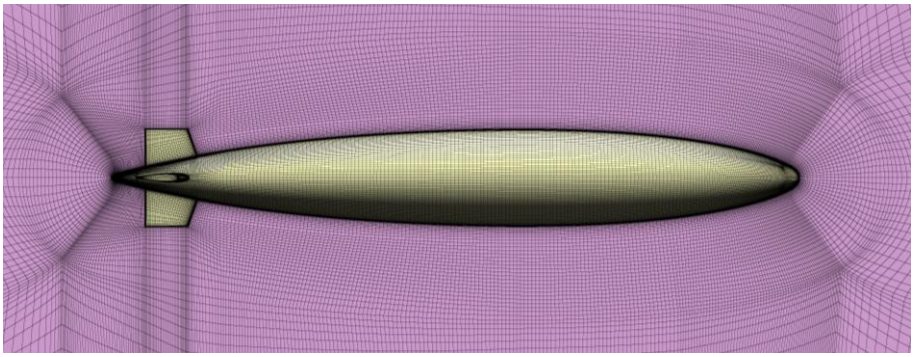

Figure 4: Surface mesh for the 11B appended Model 4621 hull and the symmetry plane mesh (every second gridline shown)

Solver

The incompressible RANS equations were solved using the ANSYS Fluent (18.1) finite volume CFD code. Both the k-ω SST and Baseline Reynolds Stress Model (BSL-RSM) turbulence closure models (TCM) were used to account for the Reynolds Stresses which arise from Reynolds averaging. Simulations using the BSL-RSM model were initialized from the corresponding k-ω SST solution to improve solution convergence and reduce computational requirements. First order discretization was used to establish the solution for the first 500 iterations. Second

order discretization was then applied for all flow and turbulence quantities until convergence of the X and Z forces was achieved.

GRID CONVERGENCE STUDY

A grid convergence study was conducted for the 11B configuration. As the unappended hull and the 3B configuration used similar mesh topology and cell sizes, the grid convergence results for the 11B configuration were assumed to apply.

Three grids of increasing resolution were considered. The relative edge length and cell count for the three grids is shown Table 2. The grid refinement study considered the body at 2° pitch as this condition was critical for the determination of the ACS lift curve slope. The grid convergence study considered only the k-ω SST TCM and grid independence was assumed to apply to simulations using the BSL-RSM TCM.

Table 2: Relative edge length and cell count for the 11B appended Model 4621 hull grid convergence study.

Grid No.	Relative Edge Length	Cell Count ($\times 10^6$)
1	1.000	20.6
2	0.794	41.7
3	0.630	82.8

The percentage variation in Z' relative to the finest grid as a function of relative edge length is shown in Figure 5. The percentage variation decreased with increasing mesh resolution.

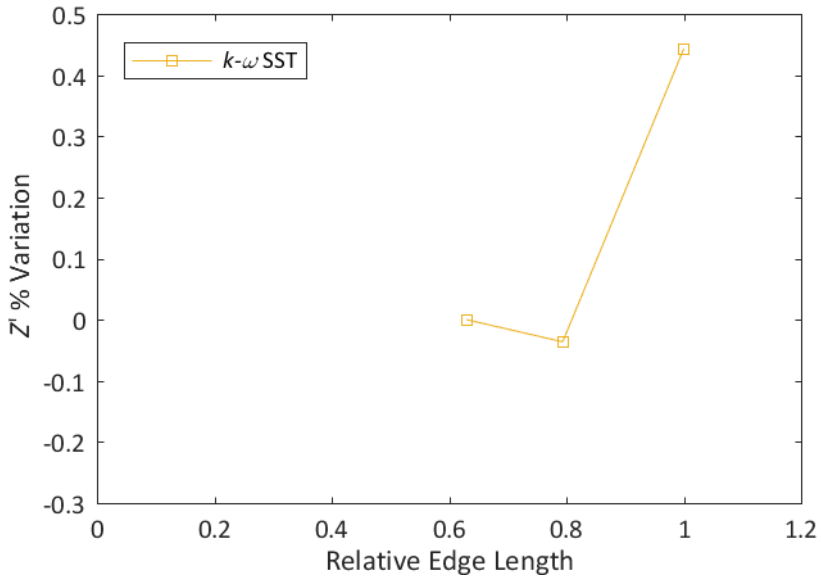

Figure 5: Percentage variation in normal force coefficient relative to finest grid

The percentage change in Z' from the coarsest to finest grid was 0.44%. Given that the error due to discretization was small relative to the large variations in ACS efficiency predicted by the Lyons and Bisgood [1] and Dempsey [2] methodologies it was decided to use the coarsest grid for subsequent simulations. Use of the coarsest grid enabled a larger parameter space to be considered with the available computational resources and time.

RESULTS

Normal Force

The CFD results for the k-ω SST and BSL-RSM TCMs were compared to Dempsey's [2] experimental results at various pitch angles to assess their accuracy. An assessment of TCM validity was made for both the unappended hull and 11B geometries.

The results of the validation study are shown in Figure 6 and Figure 7 for the unappended hull and 11B geometries respectively. Both TCMs captured the general evolution of hull normal force with angle of attack, however differences in absolute loading were seen.

For the unappended hull simulations both TCMs under predicted the normal force relative to Dempsey 's [2] experimental measurements for all pitch angles. At 2° angle of attack the k-ω SST model under predicted hull normal force by 15.9% compared to a 2.7% under prediction for the BSL-RSM TCM. This general trend was observed throughout the range of pitch angles assessed.

The calculation of ACS efficiency is dependent on the value of $C_{z,\propto}$ for both the appended and unappended configurations (see equation (4)). Consequently the large under prediction of $C_{z,\propto}$ for the unappended hull by the k-ω SST TCM results in significant over prediction of ACS efficiency (57%) relative to both the experimental data (47%) and the BSL-RSM TCM (53%). This result is in agreement with the conclusion of Phillips, Turnock and Furlong [8] which found that the BSL-RSM model is the most appropriate TCM for prediction of axisymmetric body loads. It also highlights the importance of TCM choice even at low angles of attack.

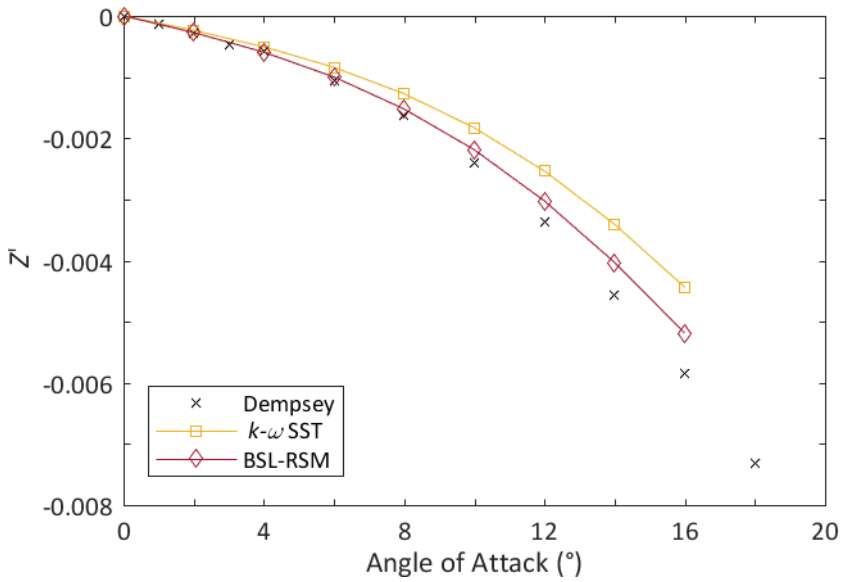

Figure 6: Variation of normal force with pitch angle for unappended Model 4621 hull.

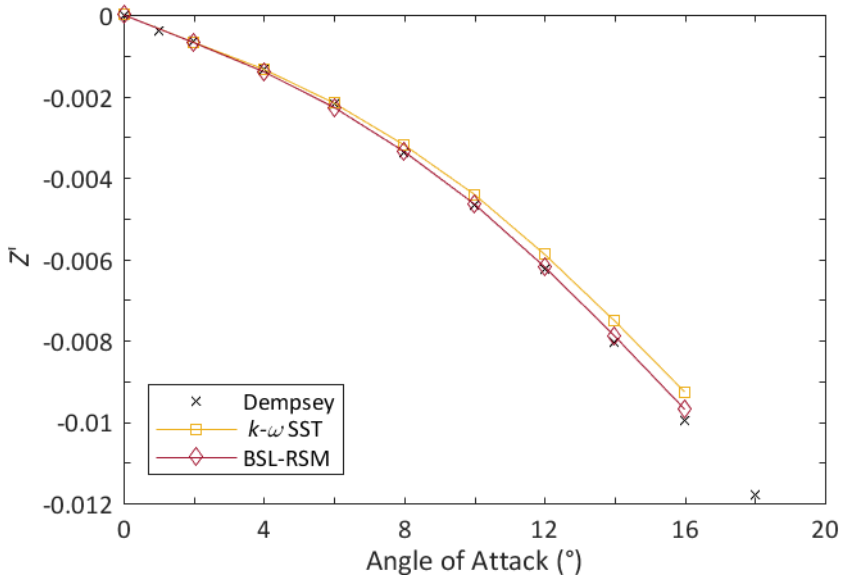

Figure 7: Variation of normal force with pitch angle for the 11B appended Model 4621 hull.

For the 11B configuration, both TCMs provided accurate predictions of the normal force up to pitch angles of approximately 6° compared to Dempsey [2] (see Figure 7). For the 11B configuration, the relative contribution of the axisymmetric body to the total normal force is reduced. Therefore, errors predicting axisymmetric hull loads are less apparent. This suggests that both models are adequate for predicting the ACS and hull normal force at low angles of attack. At pitch angles greater than approximately 6° both TCMs under predict the normal force as the axisymmetric body makes a larger contribution to total loading. At these higher pitch angles the BSL-RSM model demonstrated increased accuracy due to its improved prediction of the flow field around the axisymmetric body [8] as shown previously. This again highlights the importance of the TCM selection; however the results for high angles of attack are not relevant to the calculation of $C_{z,\propto}$ and ACS efficiency as the normal force curve slope was calculated between 0° and 2°.

Based on the results of the normal force study it was concluded that the baseline BSL-RSM turbulence model offered better prediction of the hull normal forces for both the appended and un-appended configurations. As a result it was expected that the BSL-RSM TCM would provide a better prediction of ACS efficiency. In addition, the validation study highlights the importance of turbulence model selection for accurate prediction of ACS loads and vehicle stability coefficients.

Displacement Thickness

At low angles of attack, the differing normal force predictions by the two TCMs for the unappended hull, and consequently $C_{z,\propto}$, was attributed to different boundary layer profiles and displacement thickness. Examination of surface wall-friction for both TCMs at 2° pitch did not show any flow separation from the hull; thereby discounting separation effects as the cause of reduced normal force.

The cumulative summation, from the bow to the stern, of the pressure force in the z-direction acting on the unappended Model 4621 hull (Figure 8) indicated that both TCMs gave similar force predictions over the forward section of the hull. However, the k-ω SST TCM predicted a

greater positive normal pressure force over the aft section of the hull, leading to an overall smaller normal force for the unappended hull. This indicates differences between the two TCMs prediction of boundary layer growth in the adverse pressure gradient at the stern.

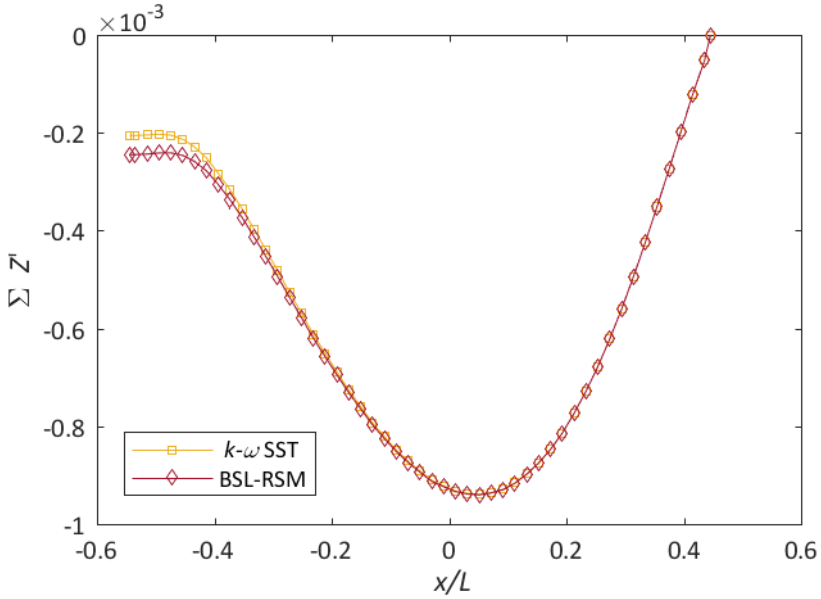

Figure 8: Cumulative summation (bow to stern) of the z-direction pressure force acting on the unappended Model 4621 hull.

The different prediction of the adverse pressure gradient was assumed to result in a different displacement thickness, and hence a different effective unappended hull shape. The displacement thickness, δ_1, was calculated as,

$$\delta_1 = \int_{s=0}^{s_e} \left(1 - \frac{u_p(s)}{u_i}\right) ds \tag{8}$$

where u_p is the velocity at a distance, s, normal to the wall and projected in the direction of u_i and u_i is the velocity of the inviscid flow past the unappended hull, which was determined from a separate inviscid simulation. The integral was computed from the wall at s = 0 to the edge of the boundary layer, s_e, which was defined as the distance where u_p was equal to 99% of u_i.

The azimuthal displacement thickness was calculated for both TCMs at x/L = -0.454 and is shown in Figure 9. The k-ω SST TCM predicted a thinner δ_1 over the high pressure side of the hull until the upper octant where it predicted a thicker δ_1. The net effect of this difference for the k-ω SST TCM was to create an effective hull shape with increased reflexive camber at the stern, relative to that from the BSL-RSM TCM. This effective hull shape resulted in reduced normal force and consequently increased $C_{z,\propto}$, compared to both Dempsey [2] and the BSL-RSM TCM.

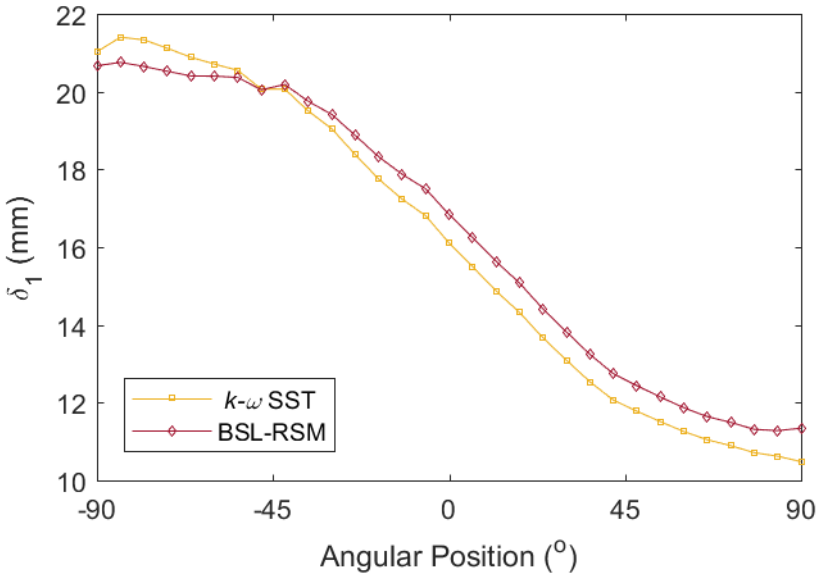

Figure 9: Azimuthal variation of the displacement thickness at x/L = -0.454 of the unappended Model 4621 hull for k-ω SST & BSL-RSM TCM.

Lift Curve Slope and Efficiency

The lift curve slope and ACS efficiency for both TCMs are shown in Table 3 & Table 4 respectively. BSL-RSM TCM accurately predicted the value of $C_{z,\propto}$ for the bare hull to within 3% of Dempsey's result. The BSL-RSM TCM also provided an accurate prediction of lift curve slope for the 3B and 11B geometries with the relative difference to Dempsey's experimental results less than 5% in both instances.

Table 3: Lift curve slope (rad^{-1}) for the unappended and appended Model 4621 hullform.

Configuration	Dempsey [2]	k-ω SST	BSL-RSM
Unappended	-0.008021	-0.006743	-0.007802
3B	-0.01518	-0.01496	-0.01569
11B	-0.01862	-0.01937	-0.01955

Table 4: ACS efficiency for the appended Model 4621 hullform.

Configuration	Dempsey [2]	k-ω SST	BSL-RSM
3B	50%	57%	55%
11B	47%	57%	53%

$C_{Z,\alpha}$ for the 3B and 11B configurations are plotted as functions of the ACS aspect ratio in Figure 10. Results for the BSL-RSM TCM are plotted together with $C_{L,\alpha}$ for an isolated ACS using the Whicker and Fehlner relationship in equation (3), $C_{Z,\alpha}$ assuming an ACS efficiency as predicted by Lyons and Bisgood [1], and Dempsey's [2] B span data points and proposed fit. The BSL-RSM results are in general agreement with Dempsey's fit, with the CFD predicting a slightly greater ACS efficiency relative to the experimental data.

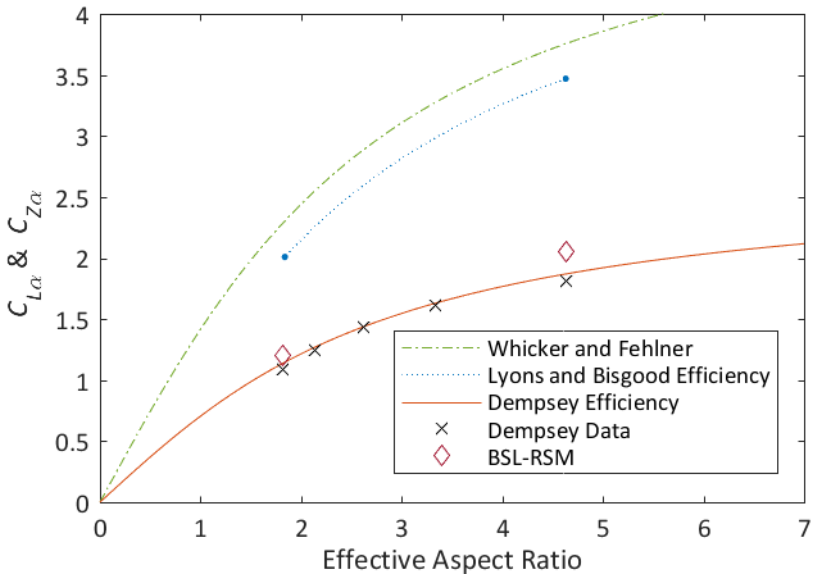

Figure 10: $C_{Z,\alpha}$ for 3B & 11B appended Model 4621 hull.

The BSL-RSM results, whilst not in absolute agreement with the proposed fit of Dempsey [2] are more closely aligned with Dempsey [2] as opposed to the equivalent prediction of Lyons and Bisgood [1]. For the 3B and 11B configurations , the Lyons and Bisgood [1] method predicts an ACS efficiency of 87% to 92% respectively as shown in Figure 10. The results of the CFD simulations provide strong evidence for the validity of the Dempsey [2] experiment and that the Dempsey [2] efficiency prediction is suitable for use at model scale.

Furthermore, solutions to the RANS equations assume a turbulent flow field. This assumption, together with the CFD results being in strong agreement with the experimental results for ACS efficiency suggests that any underestimation of tailplane efficiency is not attributable to laminar flow.

Reynolds Number Dependence

To investigate Reynolds number dependency, the flow over the 3B and 11B geometries was simulated at increased inlet velocities to simulate higher Reynolds numbers. The Reynolds numbers simulated encompassed the range that could be expected between model scale testing and a full scale submarine.

The results of this analysis are shown in Figure 12. In addition to the CFD model data, equivalent simulations for a geometry based on the DST generic BB2 submarine geometry [9] have been included. The BB2 hull has an L/D of 7.31 and an ACS aspect ratio of 4. The BB2 geometry was modified to match the configuration of Dempsey [2], i.e. the ACS layout was changed from an X-plane configuration to a cruciform arrangement, and the vertical rudders, sail, and casing were removed. The BB2 ACSs were designed within the hull bounding box and so rotation of the ACS by 45° to the cruciform configuration results in a larger span relative Dempsey's B span. This modified geometry is herein referred to as "mod-BB2" and is shown in Figure 11. Results for the mod-BB2 geometry were computed using a similar grid and solution methodology to the Dempsey simulations presented.

Figure 11: Plan and elevation views of the mod-BB2 geometry.

It is clear from Figure 12 that ACS efficiency is strongly influenced by Reynolds number. The ACS efficiency of both the Dempsey [2] and mod-BB2 geometries increased with Reynolds number. The mod-BB2 ACS efficiency increased more rapidly and attained a higher efficiency at full scale Reynolds numbers. The more rapid increase in ACS efficiency observed for the mod-BB2 might be due to the steeper stern half angle (16^o for mod-BB2) relative to that of the Dempsey [2] (6.5^o) geometry. The more rapid increase in efficiency might also be due to the increased span of the mod-BB2 geometry relative to Dempsey's B span.

ACS efficiency increases continuously with Reynolds number and critical/sub-critical behaviour was not observed. ACS efficiency appears to be independent of aspect ratio at higher Reynolds as both the 3B and 11B geometries converged to similar efficiencies at full scale Reynolds numbers, although this requires further simulations to verify.

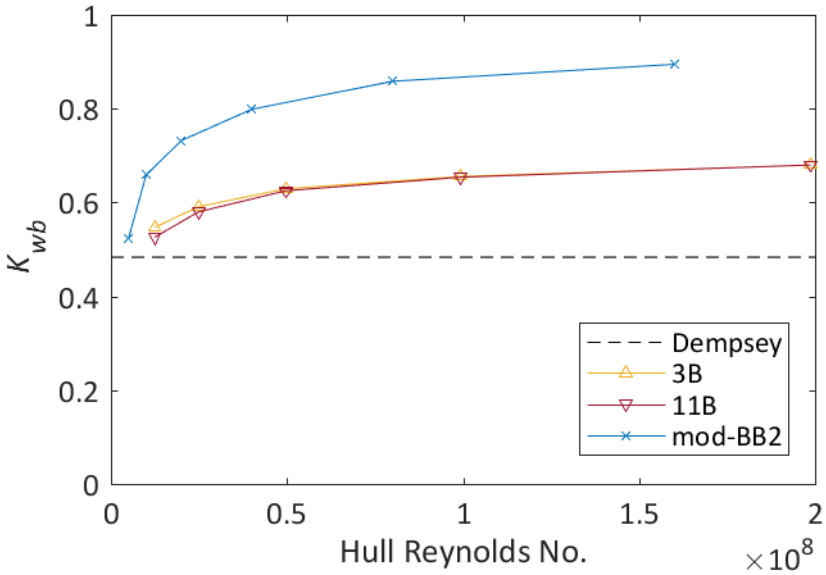

Figure 12: ACS efficiency variation with Reynolds Number for the appended Model 4621 hull and mod-BB2.

Mackay, Watt and Bohlmann [4] suggested that the increased efficiency as a function of Reynolds number is due to the effect of Reynolds number on the boundary layer thickness. The boundary layer thickness decreases with Reynolds numbers. At full scale the boundary

layer at the ACS would be relatively thinner than at model scale, with an equivalent decrease in the momentum thickness. The reduced momentum thickness would result in a smaller proportion of the ACS span being influenced by the reduced velocity, low energy boundary layer and is therefore able to produce greater normal force. To confirm this, further investigation of the change in momentum thickness with Reynolds number is required.

CONCLUDING REMARKS

RANS CFD was used to numerically model the experiments of Dempsey [2]. Good agreement between the CFD model and experimental data was observed for the two different ACS geometries studied.

Both the k-ω SST and BSL-RSM TCMs were suitable for prediction of absolute normal loads for appended axisymmetric bodies. However the k-ω SST was found to be unsuitable for the prediction of loads for the unappended axisymmetric body at low (2^o) pitch angles and is therefore unsuitable for prediction of ACS efficiency. This limitation was attributed to the k-ω SST TCM's different prediction of the adverse pressure gradient in the aft portion of the hull and consequently a different displacement thickness and equivalent hull shape.

The use of RANS CFD, which assumes fully turbulent flow, indicates that the reduced ACS efficiency of Dempsey's [2] experiments is not due to laminar boundary layer effects. Clear critical/subcritical ACS efficiency was not seen. However significant Reynolds number dependence was observed between model scale and full scale. It was suggested that this dependency was the result of the smaller boundary layer thickness at higher Reynolds numbers and therefore a greater proportion of the ACS span being subjected to the higher freestream velocity resulting in a greater normal force.

The CFD results confirms the suitability of using Dempsey's [2] data for predicting ACS efficiency at model scale Reynolds numbers and for geometries with relatively shallow stern angles. It highlights some of the limitations of empirical methods for calculating hydrodynamic coefficients and reinforces the importance of Reynolds number and geometry equivalence when applying empirical methodologies.

REFERENCES

[1] D. J. Lyons and P. L. Bisgood, "An Analysis of the Lift Slope of Aerofoils of Small Aspect Ratio, Including Fins, with Design Charts for Aerofoils and Control Surfaces," 1950.

[2] E. M. Dempsey, "Static Stability Characteristics of a Systematic Series of Stern Control Surfaces on a Body of Revolution," Bethesda, 1977.

[3] M. C. Bettle, "Validating Design Methods for Sizing Submarine Tailfins," in *Warship 2014: Naval Submarines & UUV's*, 2014.

[4] M. Mackay, G. D. Watt, and H.-J. Bohlmann, "Modeling Submarine Tailplane Efficiency," in *RTO SCI Symposium*, 2002.

[5] L. Whicker and L. Fehlner, "Free-Stream Characteristics of a Family of Low-Aspect Ratio, All-Movable Control Surfaces for Applications to Ship Design," Washington D.C., 1958.

[6] M. Renilson, *Submarine Hydrodynamics*, 2nd ed. Springer International Publishing, 2018.

[7] C. G. Armstrong, H. J. Fogg, C. M. Tierney, and T. T. Robinson, "Common themes in multi-block structured quad/hex mesh generation," in *24th International Meshing*

Roundtable (IMR24), 2015.

[8] A. B. Phillips, S. R. Turnock, and M. Furlong, “Influence of turbulence closure models on the vortical flow field around a submarine body undergoing steady drift,” *J. Mar. Sci. Technol.*, vol. 15, no. 3, pp. 201–217, 2010.

[9] B. Overpelt, B. Nienhuis, and B. Anderson, “Free Running Manoeuvring Model Tests On A Modern Generic SSK Class Submarine (BB2),” in *Pacific International Maritime Conference*, 2015.